LAWRENCE
LIVERMORE
NATIONAL
LABORATORY

LLNL-JRNL-457059

The Consequences of Interface Mixing on Organic Photovoltaic Device Characteristics

D. Huang, S. A. Mauger, S. Friedrich, S. J. George, D. Dumitiu-LaGrange, S. Yoon, A. J. Moule

September 27, 2010

Advanced Functional Materials

Disclaimer

The Consequences of Interface Mixing on Organic Photovoltaic Device Characteristics

By David M. Huang[b], Scott A. Mauger[a], Stephan Friedrich[c], Simon J. George[d], Daniela Dumitriu-LaGrange[a], Sook Yoon[a], and Adam J. Moulé[a*]

[a] Prof. A. J. Moulé, Scott A. Mauger, Dr. D. D. LaGrange, Dr. Sook Yoon
Chemical Engineering and Materials Science Department
University of California, Davis, CA 95616, USA
E-mail: amoule@ucdavis.edu
[b] Dr. David M. Huang
School of Chemistry & Physics
The University of Adelaide
SA 5005, Australia
[c] Dr. Stephan Friedrich
Lawrence Livermore National Laboratory
7000 East Ave., L-188
Livermore, CA 94550, USA
[d] Dr. Simon J. George
Advanced Biological and Environmental X-ray Facility
Lawrence Berkeley National Lab
1 Cyclotron Road Mail Stop 6R2100
Berkeley, CA 94720, USA
[*] Prof. A. J. Moulé - To whom correspondence should be addressed

Keywords: Photovoltaic Devices, Solar Cells, Conducting Polymers, Organic Electronics, Charge Transport

Abstract

Organic bulk-heterojunction solar cells are being developed as a low-cost alternative to inorganic photovoltaics. A key step to producing high efficiency bulk-heterojunction devices is film curing using either heat or a solvent atmosphere. All of the literature examining the curing process have assumed that improvement of the bulk-heterojunction morphology is the reason for the increased filling factor, short-circuit current density, and efficiency following heat or solvent treatment. We show in this article that heat treatment causes the donor polymer (P3HT) and polymer electrode (PEDOT:PSS) to mix physically to form an interface layer. This interface layer is in part responsible for the improved filling factor and strongly affects the open-circuit voltage by limiting the dark current. This result implies that a simplistic description of the P3HT/PEDOT:PSS contact as a sharp interface between bulk P3HT and bulk PEDOT:PSS cannot adequately capture its electrical characteristics.

1 Introduction

The study of organic photovoltaic (OPV) materials and devices is a quickly growing scientific field that is gaining increasing technological relevance. A recent NREL cerified power conversion efficiency (PCE) record of 8.13% was reported in the summer of 2010.[1] Efficiency records such as these show that the OPV technology is increasingly capable of competing with other thin-film PV technologies. However, many questions about the basic physics of device function still persist.

Polymer-based solar cells consist of several polymer, copolymer, and mixed polymer/fullerene layers with thicknesses less than 100 nm, as shown in Figure 1. Since the layers are so thin, the properties of the interfaces dominate the electrical function of the layers. For this reason, an understanding of the interface morphologies of the polymers used in these devices is needed. There are two types of interfaces in a bulk-heterojunction (BHJ) OPV device. First and most studied are the interfaces between the donor and acceptor materials in the BHJ layer. The mixture of poly(3-hexylthiophene) (P3HT) mixed with [6,6]-phenyl-C_{61}-butyric acid methyl ester (PCBM) is the most studied BHJ layer material. One of the large concerns in recent years has been control of layer morphology in bulk-heterojunction (BHJ) mixtures of donor-polymers with fullerene acceptors. It has been shown by numerous groups that the use of thermal treatment, solvent soaking, or non-solvent additives can greatly improve the PCE by curing the BHJ morphology.[2–4] For BHJ layer composed of P3HT mixed with PCBM, curing the BHJ layer results in increased domain size, hole mobility, and crystallinity of the P3HT.[5–7] All of the articles discribing the effects of curing the morphology have assumed that changes to the BHJ morphology and resulting electronic changes are the sole reason for changes to the device properties.

The BHJ layer is typically coated onto a substrate of indium-tin oxide with a thin layer of poly(3,4-ethylenedioxythiophene):poly(styrenesulfonate)) (PEDOT:PSS) on top. PEDOT:PSS is used as the polymer anode in virtually all organic light-emitting diodes (OLEDs) and organic photovoltaics (OPV). This electrode material is so widely used because it is insoluble in organic solvents, has a well-defined work function (Φ) of around 5.1 eV,[8] is a hole conductor, and forms an ionomer, so the dopant PSS^-

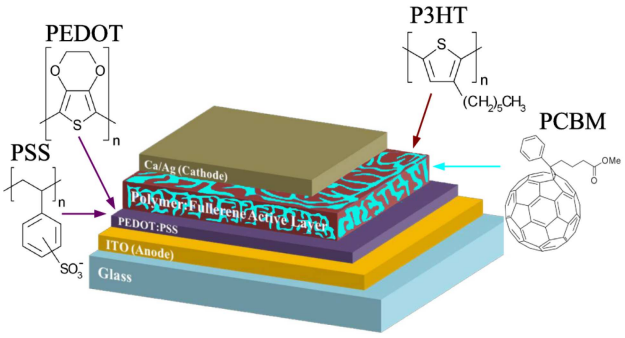

Figure 1: Schematic of typical polymer solar cell with (from top to bottom) a Ca/Ag cathode, a polymer:fullerene active layer consisting of a mixture of P3HT (electron donor) and PCBM (electron acceptor), a PEDOT:PSS hole-transporting layer, and an ITO anode on a glass substrate.

does not separate from the PEDOT matrix due to Coulombic attraction.[9] There is experimental evidence that, when spin coated in air, PSS and PEDOT forms vertically segregated layers with PSS at the top surface.[8] Further research in this area has shown that PEDOT:PSS microdomains form that are rich in PEDOT near the center and have little PEDOT at the surface. Upon heating, the PEDOT-rich domains form lateral (in plane) domains that are much more higly conductive than perpendicular to the film surface.[10–12] The second type of interface in a BHJ OPV device is an interface between material layers such as the PEDOT:PSS layer and BHJ layer. It is this second type of interface that will be the main subject of this article.

PEDOT:PSS is considered metallic because it has a continuous density of the states at the Fermi level.[13, 14] Unlike a typical metal, PEDOT:PSS does not have a large free electron density and so the Φ on PEDOT:PSS does not change greatly with contact to other materials, i.e. large dipole layers do not form.[15, 16] One interesting phenomenon with BHJ OPV devices on PEDOT:PSS layers is that the PEDOT:PSS is able to accept holes from nearly any polymer, regardless of the highest occupied molecular orbital (HOMO) level of the polymer. Scharber et. al. published that the open circuit voltage (V_{oc}) of BHJ OPV devices depends only on the energy gap between the HOMO of the polymer and the lowest unoccupied molecular orbital (LUMO) of the fullerene.[17] In organic light emitting diodes (OLEDs) a barrier for hole injection from the PEDOT:PSS into a polymer layer is a well-established phenomenon.[18] However, for an OPV device in which P3HT with a Φ of 4.7 eV has to inject a hole into PEDOT:PSS with a Φ of 5.1 eV the contact appears to be Ohmic and no net energy loss occurs. We will show in this article that the V_{oc} also depends on the degree of mixing between PEDOT:PSS and the BHJ polymer. We will also demonstrate that the PCE increase with heat treatment, which was previously ascribed only to an improvement in the BHJ layer morphology, also depends on the formation of a mixed interface layer. Finally we will argue that the device longevity is positively affected by the formation of a mixed interface layer.

2 Results and Discussion

2.1 Interface Characterization

In the following sections, we use contact angle measurements, X-ray absorption near edge structure (XANES), neutron reflectometry (NR), UV/VIS/NIR, and FTIR spectroscopy to confirm the presence, composition, and thickness of an interlayer that forms upon heating adjacent P3HT and PEDOT:PSS layers like those that occur in typical organic photovoltaic devices. Rather than characterize the structure of complete devices, we focus on the P3HT/PEDOT:PSS interface by preparing samples comprising a layer of P3HT deposited on a layer of PEDOT:PSS on a glass or silicon substrate. Mixtures of P3HT/PCBM or pure P3HT on PEDOT:PSS give identical results for all of the tests relating to formation of the interface layer, so for simplicity, only P3HT will be listed. Samples were subjected to different heat-treatment temperatures and washed repeatedly with chlorobenzene, in which P3HT is soluble, in order to determine whether any sort of physical or chemical bonding between P3HT and PEDOT:PSS takes place upon heat treatment. A similar but less well-characterized layer has previously been fabricated for hole injection layers on PEDOT:PSS surfaces for OLED applications.[19]

2.1.1 Contact Angle

The large difference between the hydrophobicities of P3HT and PEDOT:PSS makes contact angle measurements a sensitive probe of the presence of these materials at a surface that may consist of one or both of these two components. To confirm the presence of an interlayer at the PEDOT:PSS/bulk-heterojunction interface, a series of bilayer samples were fabricated. These samples were heated to various temperatures and then the P3HT was washed off using chlorobenzene. Figure 2 shows the contact angle θ_c of a water droplet on films of PEDOT:PSS, P3HT on PEDOT:PSS, and P3HT on PEDOT:PSS washed with chlorobenzene after heat treatment, versus the heat-treatment temperature. As shown in Figure 2, the contact angle of P3HT (i.e. P3HT on PEDOT:PSS) is the same (107°) for heat treatment at room temperature and 180°C. This contact angle was therefore assumed to be constant over the temperature range studied. On the other hand, the contact angle of PEDOT:PSS decreases slightly from 15° to 5° with increasing heat treatment temperature from room temperature to 180°C. This behavior could be due to an increasing predominance of the more hydrophilic PSS^- at the surface as a result of thermal annealing. For the heat-treated samples with P3HT on PEDOT:PSS washed with chlorobenzene, the contact angle

shows a distinct transition around 150°C from a contact angle similar to that of PEDOT:PSS to one resembling that of P3HT, indicating the presence of a P3HT surface layer for the washed samples heated above 150°C.

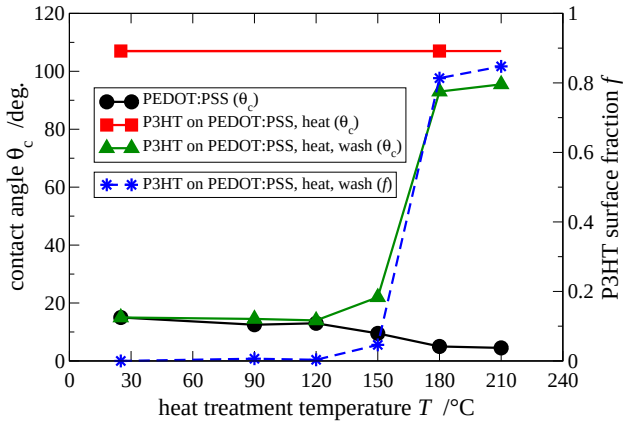

Figure 2: Contact angle (measured at room temperature) of a water droplet on films of PEDOT:PSS (circles), P3HT on PEDOT:PSS (squares), and P3HT on PEDOT:PSS washed with chlorobenzene after heat treatment (triangles) vs heat-treatment temperature. Also shown (stars) is the fraction f of the surface covered by P3HT on the washed samples estimated from Equation (1).[20]

To quantify the presence of P3HT at the interface, the fraction f of the surface covered by P3HT on the washed samples was estimated at each temperature T using the Cassie–Baxter equation [20],

$$\cos\theta_c = f\cos\theta_{\mathrm{P3HT}} + (1-f)\cos\theta_{\mathrm{PEDOT:PSS}}\,, \qquad (1)$$

where θ_{P3HT} and $\theta_{\mathrm{PEDOT:PSS}}$ are the measured contact angles of water on P3HT and PEDOT:PSS respectively. Applying this equation to the contact angle measurements (assuming that θ_{P3HT} is the same at all temperature), the surface coverage of P3HT was estimated to increase from 0 to about 5% at 150°C and then to jump to over 80% at 180°C and above, as shown in Figure 2, indicating an almost monolayer coverage at these high temperatures. This result clearly demonstrates that P3HT is tightly bound (either physically or chemically) to PEDOT:PSS upon heating to temperatures of 150°C and above, indicating the formation of an intermixed layer between the two materials. Similar contact angle experiments performed with PCBM on PEDOT:PSS showed that PCBM does not form an interlayer with PEDOT:PSS, since the contact angle was identical for PEDOT:PSS and for PEDOT:PSS that had PCBM spin-coated then washed off of it.

2.1.2 X-ray Absorption Near Edge Structure (XANES)

X-ray absorption spectroscopy is a sensitive technique to measure element-specific bonding structure. For samples much thicker than the X-ray absorption length, the absorption can be recorded by monitoring either the total electron yield (TEY) or the partial fluorescence yield (PFY) emitted from the sample in response to the core hole excitation. Since the electron escape depth of several nm is much shorter than the 1 μm escape depth for soft X-rays, TEY measurements of the X-ray absorption provide surface chemistry, while PFY measurements provide complementary information about bulk chemistry.

We have taken X-ray absorption spectra of PEDOT:PSS and P3HT samples, with and without P3HT on top, before and after heating, on the carbon K absorption edge. Figure 3 shows the surface-sensitive TEY data, while the PFY data are shown in the supporting material in Figure S1. The TEY spectra show five peaks that have been assigned as follows: 283.6 eV to the π^* of carbon that reduced by either Na^+ or H^+, 284.8 eV to the π^* that corresponds to aromatic carbon and is broadened by the C–S bond,[21, 22] 287 eV to the C–H bonds associated with the alkane chain[22] with possible contributions from the C–O bonding group[21], 288.2 eV to the π^* transition from C–H bonds associated with an aromatic ring,[22] and finally transitions >290 eV to σ^* transitions.

To differentiate between signal coming from the PEDOT and PSS polymers, we compare a samples of Na^+PSS^- (solid line) to untreated PEDOT:PSS (dashed line) and heated PEDOT:PSS (dot-dashed line) films. The Na^+PSS^- spectrum has strong features at 284.7 eV and 288.5 eV which indicate the presence of aromatic carbon and aromatic carbon hydrogen bonds, respectively. While all samples will have aromatic carbon, only PSS has a lot of C–H bonds to aromatic carbons. The heated PEDOT:PSS film also has higher intensity features at 284.7 eV and 288.5 eV than the unheated PEDOT:PSS sample. We take this as confirmation of previously reported data that shows that upon heating, the PSS moiety moves to the sample surface.[8] Supporting this data is a reduction of intensity for the 287 eV peak for heated PEDOT:PSS, which indicates reduced C–O bond and C–H (non-aromatic) character at the surface. A XANES spectrum of P3HT (dotted line) shows greatly reduced intensity for the $\pi_1^* C1s_{--\pi^*}$ peak at 284.7 eV and high intensity $\sigma^*(C--H)$ peak at 287 eV. There is no discernable peak at 288.5 eV.

Next a sample of PEDOT:PSS that has P3HT washed off after heating to a temperature of 150°C (dash dot line) was measured. For the remaining discussion this sample will be refered to as "washed". The washed sample shows peak intensity both at 287 eV and 288.5 eV. Since the 287 eV peak is associated with P3HT alkane chains and the 288.5 eV peak with the aromatic C–H bonds of PSS, it can be concluded that both P3HT and PSS are present in the top several nm of the sample surface. The peak at 284.7 eV is larger for the washed sample than for either the unheated PEDOT:PSS or P3HT. This is further confirmation of increased PSS as the surface.

The P3HT washed data is fit by numerically averaging the Na^+PSS^- and pure P3HT spectra with a 6:5 ratio. Note that this data cannot be directly compared to the surface coverage

calculated using the Cassie-Baxter equation and contact angle data because the XANES experiment has a sensitivity to a greater penetration depth at the sample surface. The fit spectra exactly reproduce the line shape and suggest that only P3HT and PSS are present at the surface and that PEDOT is not within several nm of the surface. That a numerical average of two separate spectra can be used to reproduce the washed-sample data indicates that the PSS and P3HT are forming a mixed layer, but not reacting with each other to a significant extent. A chemical reaction would cause a shift of electron density around the atoms and therefore a shift in the XANES spectrum or formation of a new peak.

The PFY spectra (Supporting imformation Figure S1) show nearly identical spectra for PEDOT:PSS with and without heating and P3HT washing. This indicates that the change in the surface has very little effect on the bulk of the film.

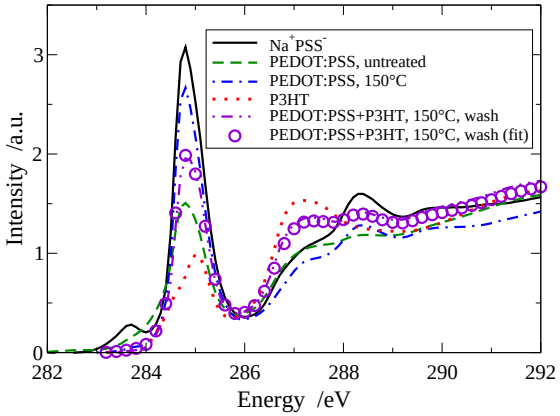

Figure 3: X-ray absorption near edge structure (XANES) spectra of the carbon K edge of Na^+PSS^- (solid line), untreated PEDOT:PSS (dashed line), PEDOT:PSS heated to 150°C (dot-dashed line), P3HT (dotted line), and P3HT on PEDOT:PSS that was heated to 150°C and then washed with chlorobenzene (dot-dot-dashed line). The points are a numerical average of the curves for the heated PEDOT:PSS film and the P3HT film with a weighting of 6:5.

2.1.3 Neutron Reflectivity

Neutron reflectivity data for selected samples are shown in Figure 4a, along with fits to the data using a slab model for the scattering length density profile of the film. The scattering length density profiles near the top (air) interface obtained from the model fitting are shown in Figure 4b for selected samples. (The neutron reflectivity data and fits and modeled scattering length density distributions for all measured samples are given in Figures S2 and S3, respectively, of the Supporting Information.) The scattering length densities of PEDOT:PSS, $\rho_{PEDOT:PSS}$, and P3HT, ρ_{P3HT}, were obtained from the fits of the neutron reflectivity data for the samples with only PEDOT:PSS and only P3HT, respectively, on silicon. The values of $\rho_{PEDOT:PSS} = 1.80 \times 10^{-6}$ Å^{-2} and $\rho_{P3HT} = 0.786 \times 10^{-6}$ Å^{-2} are consistent with those estimated using the NIST Scattering Length Density Calculator[23] from the molecular formulas of PEDOT, PSS, and P3HT and approximate densities of 1.1 g/cm^3 for these polymers of 1.68×10^{-6} Å^{-2} (assuming a 1:6 mixture of PEDOT and PSS with SLDs 1.85×10^{-6} Å^{-2} and 1.49×10^{-6} Å^{-2}) and 0.68×10^{-6} Å^{-2} respectively.

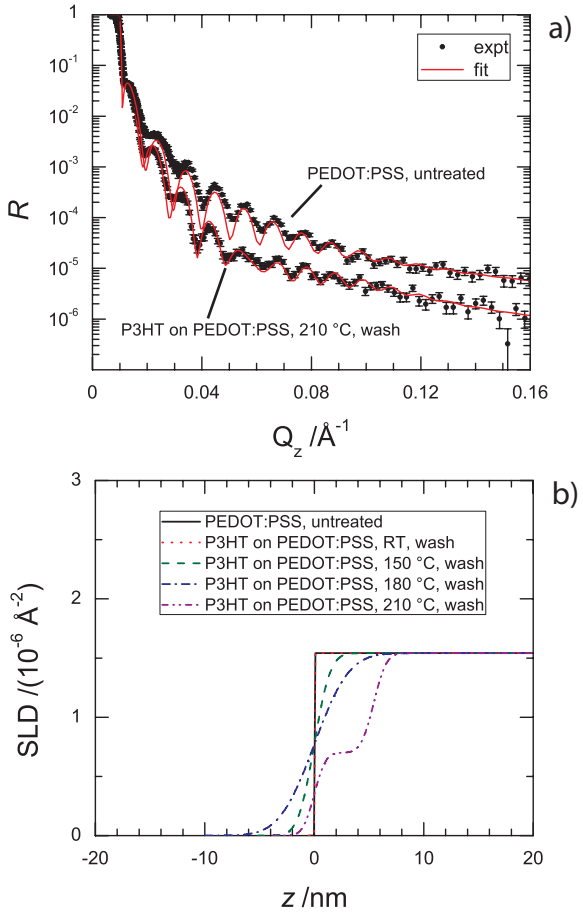

Figure 4: (a) Neutron reflectivity data (points) and model fits (lines) for an untreated PEDOT:PSS film (upper curves) and for P3HT on PEDOT:PSS heated to 210°C then washed with chlorobenzene (lower curves) (both on silicon wafer substrates). (b) Scattering length density (SLD) profiles vs distance from the top surface of the film from fits to reflectivity data for untreated PEDOT:PSS (solid line), unannealed P3HT on PEDOT:PSS washed with chlorobenzene (dotted line), and heat-treated P3HT on PEDOT:PSS washed with chlorobenzene, heated to 150°C (dashed line), 180°C (dot-dashed line), and 210°C (dot-dot dashed line) Only the region close to the top (air) interface is shown.

Figure 4b shows that scattering length density profiles of

the untreated PEDOT:PSS film and the film in which P3HT was spin-coated on to PEDOT:PSS and then washed with chlorobenzene without heat treatment are virtually indistinguishable, indicating the absence of P3HT on the latter film, which is consistent with the results of the other characterization experiments. For the films that were heat treated after deposition of P3HT on to PEDOT:PSS but before washing with chlorobenzene, the interface width (twice the "roughness" σ) is larger than that of the untreated PEDOT:PSS film and increases with temperature, from 3.4 nm for the film heated to 150°C to 6.4 nm and 7.0 nm respectively for the films heated to 180°C and 210°. The increased interface width could be due to (1) increased roughness of the interface, (2) vertical segregation of PSS and PEDOT (with PSS nearer the surface), or (3) the presence of P3HT on the surface, which could also be intermixed with PEDOT and PSS. Unfortunately, the ordering of the magnitudes of the scattering length densities, $\rho_{P3HT} < \rho_{PSS} < \rho_{PEDOT}$, makes it difficult to distinguish between these three cases. However, the absence of an increase in the measured surface roughness measured by AFM with heat treatment (not shown) allows us to rule out case (1). We also find that the fit to the neutron reflectivity data for the 210°C-heated film is noticeably improved when a several-nanometer layer of P3HT is assumed to exist on top of the PEDOT:PSS layer (as shown in Figure 4) instead of simply assuming a rough PEDOT:PSS interface. The 150°C- and 180°C-heated samples do not seem do have a distinct P3HT layer, but a thin layer with lower SLD is clearly present. When analyzed in the context of the other measurements, the neutron reflectivity results indicate that the bi-layer samples heated above 150°C form a few nanometers of P3HT intermixed PEDOT:PSS, with a predominance of PSS over PEDOT near the interface. After washing with a good solvent for P3HT this intermixed layer remains.

2.1.4 Kelvin probe force microscopy

Kelvin force probe measurements make a direct measurement of the Fermi energy of a surface.[24] The work function (Φ) of the surface, defined as the minimum energy required to remove an electron from the surface,[25] is measured using a Kelvin probe in the case when the Fermi energy lies within a partially occupied energy band. Then the Fermi energy and Φ are identical. We prepared two sets of PEDOT:PSS samples with and without P3HT coated on top. The samples were heated at temperatures ranging from room temparature to 210°C for 5 minutes. The samples were then all washed multiple times with CB. Then the Fermi energy of the samples was measured. The samples that were pure PEDOT:PSS all have continuous and partially filled density of states (DOS) at the Fermi energy, so Φ is directly measured and shows values near the literature reported value of -5.2 eV (Figure 5). Φ increases slightly with increasing heat treatment, which means that more PSS on the surface makes it more difficult to remove an electron from the surface. For the P3HT washed samples, the measured Fermi energy decreases with increasing heat treatment temperature. This result is also expected. The reported value of the oxidation potential of the P3HT HOMO level is -4.74 eV with respect to vacuum measured using cyclic voltamitry[26] and ∼4.5 eV measured using UPS.[27, 28] As P3HT mixes with PSS the most easily removed electron comes from the HOMO of P3HT and so Φ of the surface is reduced. This change in the Φ shows that no vacuum level shift occurs at the interface between P3HT and PEDOT:PSS, as has been previously reported.[27]

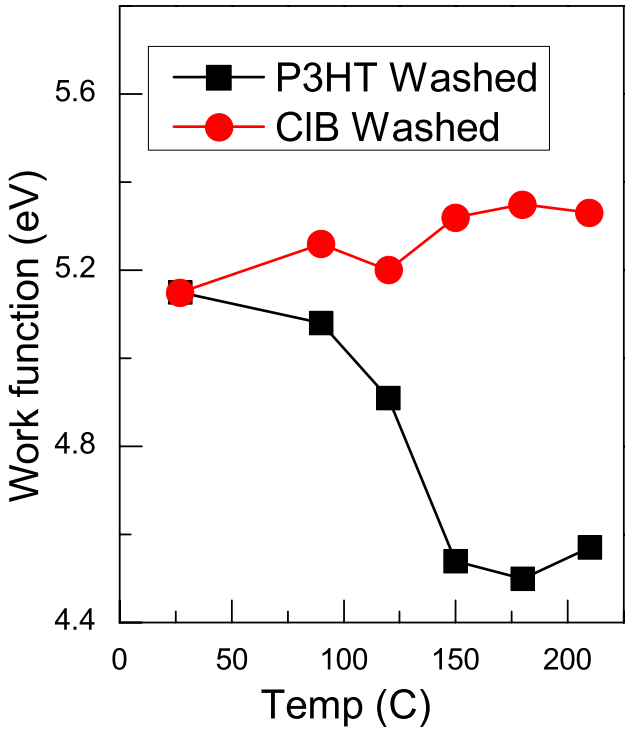

Figure 5: Work function measurements performed by Kelvin probe force microscopy of PEDOT:PSS layers that have (circles) and have not been coated with P3HT (squares).

The Φ measurements allow us to make several conclusions. First, the Φ of the mixed P3HT/PSS layer is set by the P3HT within the layer. Second, Φ is the same for mixtures of P3HT/PSS as for pure P3HT. Finally, since Φ is the same for 150°C, 180 °C, and 210°C P3HT washed samples, very little or extensive material mixing between P3HT and PSS does not significantly change the work function.

2.1.5 Mixing Mechanism

We have shown in some detail that with heating, P3HT sticks to the surface of PEDOT:PSS and that the upper surface is composed almost entirely of PSS. There are three mechanisms that can be imaginged to explain the formation of this P3HT/PSS layer. (1) P3HT chemically reacts with PSS upon heating

leading to the breaking of some conjugated bonds and the formation of new P3HT/PSS chemical bonds.

(2) P3HT physically mixes with PSS upon heating and becomes trapped in a mixed layer, but remains uncharged.

(3) P3HT physically mixes with PSS upon heating and becomes oxidized to $P3HT^+$.

Possibility (1) is unlikely because there is no evidence of the formation of new bond types in the XANES data (Figure 3). We further tested whether new bonds form by comparing FTIR plots (Supporting Information Figure S4) of ground powder mixtures of PEDOT:PSS and P3HT before and after heating to 180°C for one hour. Comparison of the two spectra show essentially identical peak ratios for all bond types. We expect that the most likely possible reaction is an acidic attack of the thiophene ring of P3HT by the HSO_3 group of PSS. If this reaction occured a new peak at 2535 cm^{-1} would appear for a S–H bond.[29] Since this peak is absent, we conclude that no chemical reaction occurs between P3HT and PSS upon heating.

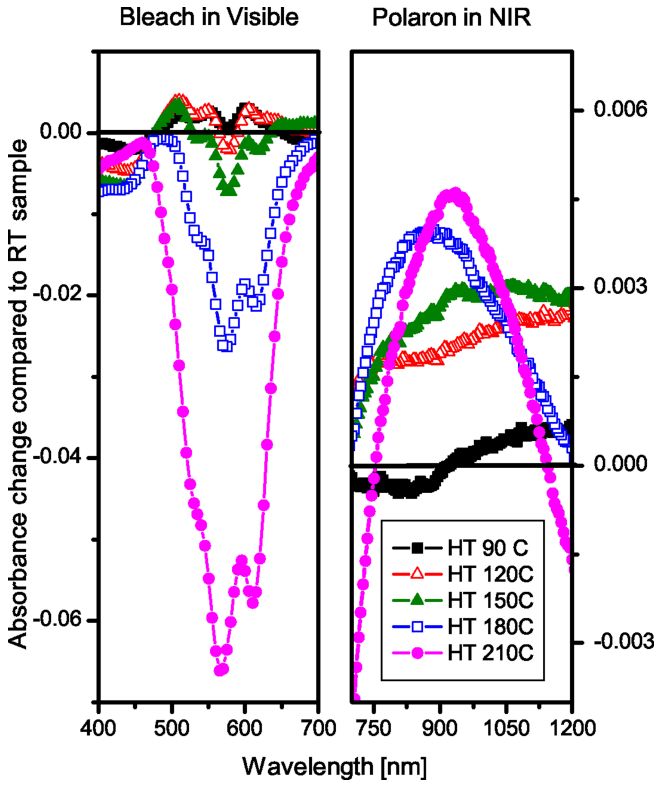

Figure 6: UV/VIS/NIR difference spectra of bi-layer samples of PEDOT:PSS/P3HT heated to 90°C, 120°C, 150°C, 180°C, and 210°C.

Since no new bond types appear to be forming we now attempt to determine whether possibility (2) or possibility (3) cause P3HT to become insoluble upon heating the PEDOT:PSS/P3HT bi-layer. The only realy difference between the two possibilities is to determine whether the P3HT becomes oxidized by the PSS or whether it is simple mixing of neutral species. Presented in Figure 6 are UV/VIS/NIR difference spectra for a PEDOT:PSS/P3HT film that has been treated to increasing heating temperatures. The spectra in Fig. 6a show the spectra of the heated films subtracted by the room temperature (RT) film in the visible and Figure. 6b shows the same data on a different scale in the near infrared (NIR). The spectra are displayed in this manner because separate diffraction gratings are required to cover the two measurement ranges and because $P3HT^+$ has a much lower absorbance than P3HT.

Figure 6a (visible wavelengths) shows that mild heating (up to 120°C) increases the P3HT absorption, probably due to increased ordering in the film.[30] However at higher temperatures, visible absorption increasingly bleaches. Figure 6b (NIR) shows the growth of an absorption peak centered at $\sim$ 900 nm.[31] This NIR peak has been assigned previously to $P3HT^+$.[32, 33] The fact that $P3HT^+$ is forming with increased heating is proof that the mixing is being caused by oxidation of P3HT in the mixed layer. PSS is unconjugated and so does not transport charges. This means that the oxidized P3HT at the interface is the only charge carrier. The presence of an oxidized P3HT layer suggests that hole transport is even more strongly selected at this interface than it would be without the mixed layer because the charge transport occurs through the p-doped HOMO levels of P3HT. The data presented here does not allow us to quantify how much of the P3HT in the mixed layer is charged. The Kelvin probe measurements in Figure 5 shows that the Fermi level of the mixed layer is equivalent to the HOMO level of the P3HT. This suggests that the Fermi level is fixed within the HOMO band of the P3HT at the interface. A greater forward bias would be necessary to raise the Fermi level to within the HOMO/LUMO gap of P3HT/PCBM, respectively, than woud be required without this doped interlayer.

2.2 Electrical Effects of Interlayer Formation

A difficult problem in this study is to separate the electrical changes that come from the formation of a PSS/P3HT interface layer upon heating from the electrical effects brought about by an improved BHJ layer morphology through heating. It has been well documented that heating the mixture of P3HT/PCBM to temperatures of $\sim$150°C improves the efficiency of OPV devices,[34, 35] increases mobility of holes in P3HT,[6] increases the crystallinity of P3HT,[5] and increases the phase separation between P3HT and PCBM.[7, 34] In order to make a comparison between interlayer induced and BHJ morphology induced changes in electrical function of an OPV device we have compared devices that have been prepared with and without non-solvents that improve the morphology.[36, 37] Moulé et al. demonstrated that the morphology of P3HT:PCBM bulk-heterojunction layers can be improved in unheated layers using the non-solvent additive nitrobenzene (NB).[38] NB was shown to cause aggregation of the P3HT, which led to an im-

proved short circuit current density (J_{sc}) and filling factor (FF) compared with as-cast devices that were solution cast from solvents such as chlorobenzene (CB) and o-xylene. Further work (in preparation) has shown that the NB additive does not evaporate out of the bulk-heterojunction film, even upon heating to >150°C and that the presence of NB increases the onset of melting of the P3HT/PCBM blend by over 50°C. These circumstances mean that, in effect, the morphology of bulk-heterojunction films with NB added does not change significantly upon heating. UV/Vis and fluorescence spectra of films heated to 180°C are identical to those of as-cast films, which strongly indicates that the morphology of the film is maintained by the presence of the NB.

In this section, we compare the current density–voltage (J–V) curves of CB-cast and CB/NB-cast films that had been heated to differing temperatures. As was stated in the introduction, heating of a CB-cast P3HT/PCBM film causes aggregation, increases hole mobility, and causes a red-shift of the UV-VIS absorption spectrum. However, especially at lower temperatures, heating of the CB/NB-cast films has no effect on the layer morphology and so any observed electrical changes are isolated to changes at the interface. Using this comparison, we will show that some changes in electrical characteristics are not due to morphological changes, but rather to the formation of the mixed layer at the interface between P3HT and PEDOT:PSS that was introduced above.

Figure 7 shows J–V curves for P3HT:PCBM OPV devices cast from CB and CB/NB. The devices were measured directly after spin coating and after heating to 180°C. It can be seen that the J_{sc} and fill factor (FF) of the CB/NB-cast devices are nearly identical in the as-cast and heated devices, but that both of these characteristics increase greatly upon heating for the CB-cast device. We have already noted that the morphology of the CB/NB-cast devices does not change upon heating. The only clear change in the J–V data is an increase of the open-circuit voltage (V_{oc}) from 0.6 V to 0.66 V. By comparison, the V_{oc} of the CB-cast device drops from 0.72 V to 0.66 V upon heating. Comparison of the two device types shows that an improved morphology through heating or solvent additive usage can increase the FF and J_{sc}, but the V_{oc} is only improved using heating.

Figure 8a shows a plot of V_{oc} versus heat-treatment temperature for a series of CB- and CB/NB-cast devices, in which it can be seen that V_{oc} for both device types varies non-monotonically. V_{oc} shows a minimum at 120°C and is the same for heat-treatment temperatures above 180°C, but there is no obvious trend. A plot of the compensation voltage V_0 (the voltage at which the current–voltage curves in the dark and under illumination cross) versus heat-treatment temperature is also shown on the same axis. Heating the device up to temperatures of 180°C clearly increases V_0 for both device types. Interestingly, V_0 is nearly identical for both device types in Figure 8a as a function of the heat-treatment temperature. Figure S5 in the Supporting Information shows V_0 as a function of heat-

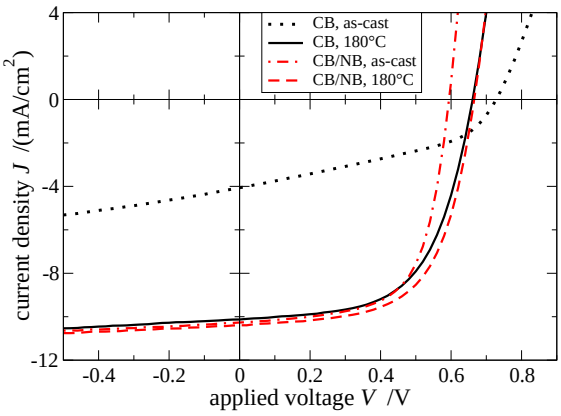

Figure 7: Current–voltage curves of 3:2 w/w P3HT:PCBM devices spin cast from chlorobenzene (CB, dotted lines: as-cast; solid lines: heat treated at 180°C) and from chlorobenzene/nitrobenzene (CB/NB, dot-dashed lines: as-cast; dashed lines: heat treated at 180°C).

treatment temperature for several other fabrication conditions. It can be seen that for all fabrication conditions, V_0 has a similar heat treatment temperature dependence.

The value of V_0 in bulk-heterojunction solar cells is the applied voltage required to compensate for the work function difference between the HOMO of the donor at the anode and the LUMO of the acceptor at the cathode.[39] Since the two device types have very different morphologies and very different J–V curves for most of these temperatures, we must conclude that something in addition to the bulk-heterojunction layer controls V_0. V_0 can be changed by the effects of band bending, formation of an interface dipole layer or doping of the material at the interface. Correlation of the heat-treatment temperature-dependence of the V_0 with the temperature dependence of the P3HT/PSS interlayer formation indicates that the increased V_0 is due to the formation of the PSS/P3HT interlayer.

Given this very clear picture of a P3HT/PSS interlayer, we ask how do the electrical properties of the device change because of this layer formation. PSS is an insulator. It can be assumed that the charge transport through the ∼3–7 nm thick interlayer occurs through the P3HT. Small-molecule OPV devices are fabricated with a donor/mixed/acceptor layer structure in order to increase the selectivity of charge transport to the two electrodes.[40] The increased compensation voltage V_0 with the formation of the interlayer, shown in Figure 8a, is indirect evidence of increased electrode selectivity for holes. The use of a PEDOT:PSS replacement anode composed of a blend of 4,4'-bis[(p-trichlorosilylpropylphenyl)-phenylamino]biphenyl ($TPDSi_2$) poly[9,9-dioctylfluorene-co-N-[4-(3-methlypropyl)]-diphenylamine (TFB) has also been shown to offer greater hole solectivity than PEDOT:PSS.[41]

Figure 8b shows the short-circuit current density J_{sc} versus temperature data for both the CB- and CB/NB-cast devices.

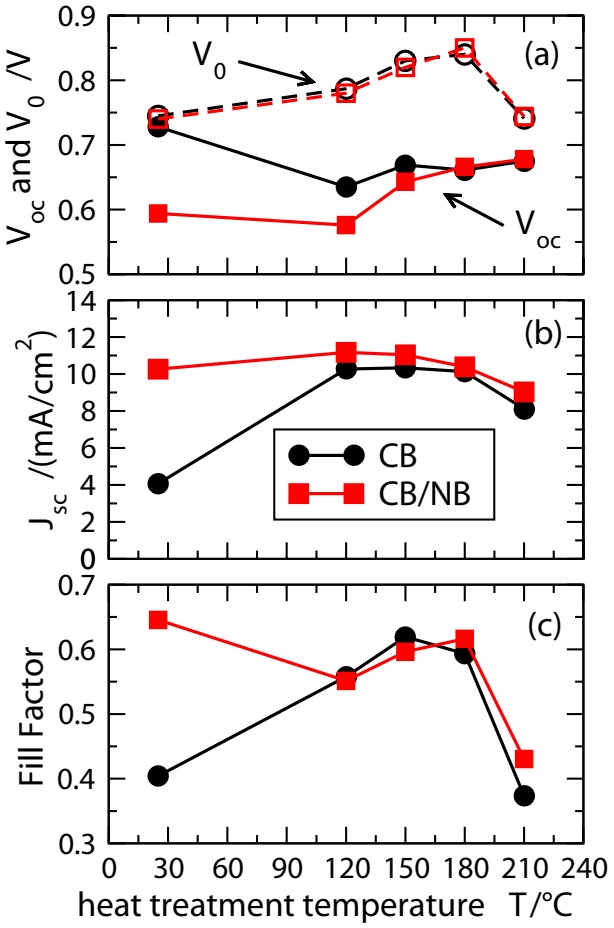

Figure 8: (a) V_{oc} (solid lines) and V_0 (dashed lines), (b) J_{sc}, and c) FF vs heat treatment temperature for P3HT/PCBM devices that were cast from CB (◯) and CB/NB (□).

Here we see that the CB/NB-cast samples have a higher J_{sc} for all heat-treatment temperatures, which can be explained by the red-shifted absorption spectrum with respect to the CB-cast samples [38], which results from an increase in the total number of photons absorbed by the CB/NB active layers even with identical layer thickness. For both device types the maximum in J_{sc} occurs with a heat treatment temperature of 120°, at which temperature a PSS/P3HT interlayer has not yet formed. The maximum occurs for this heat treatment temperature because the heating has improved the morphology and ability of the BHJ layer to absorb light. Once the interlayer forms, P3HT from the active layer becomes bleached in the visible with the formation of $P3HT^+$ in the interlayer. Figure 6 shows this bleach with the formation of the interlayer. Since the active layer absorbs less light, the J_{sc} is reduced with the formation of the interlayer.

It has been widely reported that heating a P3HT/PCBM BHJ device to a temperature of ∼150°C leads to the highest power conversion efficiency.[34, 42–44] We have shown that V_{oc} varies depending on the morphology, but is maximized by heat treatment to 180°C. The J_{sc} reaches a maximum at 120°C and is reduced with the formation of an interlayer. The filling factor (FF) seems to be most positively affeted by the formation of the PSS/P3HT interlayer. Figure 8c shows the FF versus heat-treatment temperature for both the CB- and CB/NB-cast devices. As seen in Figure 7, the FF for CB/NB-cast devices is very high for a device that is not heat-treated, while the FF for a CB-cast device is quite poor.[38] For devices heated to 120°C, the FF is identical for both device types and still low ∼0.55. This is interesting considering that the morphology of the CB/NB cast devices was already good enough for a FF of 0.66 without heat treatment and climbs back to 0.61 after heat treatment to 180°C. The morphology of the CB/NB-cast layer does not change, but the FF is reduced because the BHJ layer does not effectively inject holes into the PEDOT:PSS after heating to 120°C. We speculate that either the thickened insulating PSS layer reduces the charge transport rate, or that the orientation of the P3HT domains are ineffective for charge transport into the PEDOT:PSS.[45] With heating to higher temperatures, P3HT mixes with PSS and is oxidized to $P3HT^+$. With the formation of the mixed interlayer, the FF of devices from both casting solvents is increased to above 0.6. Finally with heating to 210°C, the FF drops down to below 0.4. The change comes from the formation of an overly thick mixed layer >10 nm (Figure S3) and breakdown of the PEDOT:PSS layer itself.[13]

There are several reasons that the formation of the mixed PSS/P3HT interlayer increases the FF. First, the formation of the mixed interlayer decreases the dark current through the device. Supporting Information Figure S6 shows the dark and light JV curves for all of the devices reported in this study. Examination of the dark JV curves shows that the dark current is somewhat reduced by the formation of the interlayer in the voltage region between 0.45 and 0.8 V. While this change is minor, it shows that the interlayer is effective in reducing the dark current. This effect would probably be much more apparent and important in devices that use ambipolar polymers.[46–48]

The data presented in the preceeding sections shows that heating of the bulk-heterojunction layer above 150°C leads to the formation of an insoluble layer that is formed from a mixture of P3HT and PSS. In several recent articles, the vertical segregation of P3HT and PCBM bulk-heterojunction layers was studied.[49–52] Most of these articles showed that the density of P3HT is higher at the air interface and lower at the PEDOT:PSS interface because segregation is driven by the difference between the surface energies of P3HT and PCBM at these two interfaces. Xu et al.[52] predicted better electronic properties for inverted devices due to the increased hole carriers near the top electrode and increased presence of electron carriers near the bottom interface. Germack et al.[49] showed identical electronic properties regardless of P3HT density near the hole-collecting electrode. In contrast, van Bavel et al. [51] showed higher P3HT density near the PEDOT:PSS electrode.

Our results may reconcile the discrepancies between these results. We show that P3HT forms an interlayer with PEDOT:PSS upon heating. All of the authors above used slightly different preparation proceedures for their bulk-heterojunction layers, including different heating times and temperatures. Using contact angle measurements of washed films we have shown that PCBM does not stick to or mix with PEDOT:PSS at all measured temperatures. We have shown conclusively that P3HT forms an interlayer with PEDOT:PSS upon heating. We make no speculation about the vertical composition of P3HT and PCBM within the layer, but at the hole-collecting electrode, our results suggset that PCBM is excluded from the interface with the hole-collecting electrode for heated bulk-heterojunction layers. This finding, in combination with the results of Germack et. al. that showed that the OPV device efficiency was very insensitive to vertical segregation, suggests that the formation of a mixed interface layer will increase the longevity of the device. It is well known that a PV device will heat cycle during the day with temperatures up to 80°C and that the morphology of P3HT/PCBM can be changed by these temperatures.[35] The FF data presented on CB/NB cast devices in Figure **??**c shows that even a BHJ layer with good morphology can have a poor FF due to poor interface charge transfer. The formation of the mixed interlayer at high temperatures assures good hole conduction at this interface. An interface formed from an inorganic hole conductor will not fix the P3HT at the interface and so will be more subject to material instability.

3 Conclusions

In conclusion, we have shown that heat treatment of P3HT/PCBM bulk-heterojunction layers that are deposited onto PEDOT:PSS hole transoprt layers leads to material mixing of the layers. Specifically, at temperatures at and above 150°C the P3HT forms an interlayer with PSS from the PEDOT:PSS. This mixed interlayer forms to a thickness of 3-5 nm and is composed of a mixture of $P3HT^{+}$ and PSS^{-}. After formation, the mixed interlayer is insoluble to both organic solvents and to H_2O. The oxidized P3HT is the charge carrier and since it is doped, it is very selective to hole transport. The work function of the mixed interlayer is nearly identical to the HOMO level of the P3HT, which indicates p-doping of the P3HT. Examination of the heat treatment temperature dependence of devices that were fabricated with differing morphologies shows that the formation of the mixed interlayer changes the compensation voltage most strongly and predictably. The mixed interlayer reduces the dark current under applied bias and so has the effect of improving the filling factor and V_{oc} of the device. Finally, once the mixed interlayer has formed, the composition and interaction of the P3HT with the PEDOT:PSS layer does not change with heating. We showed that heating to temperature below 150°C for high-efficiency devices degrades the device performance. The presence of the interlayer will therefore increase the device lifetime because it eliminates orientation dependence at the anode interface.

4 Experimental

Materials and Device Fabrication: All devices were fabricated on indium tin oxide (ITO) glass slides that had been etched with acid to a specified shape using a mask. The substrates were then cleaned in an ultrasonic bath with chloroform, acetone, mucasol, and deionized water. Prior to spin coating a ∼40 nm polyethylenedioxythiophene:polystyrenesulphonate (PEDOT:PSS; H.C. Starck) layer, the ITO substrates were placed in an ozone plasma for 30 min. The PEDOT:PSS-coated films were dried at 110°C for 3 min and then immediately taken into an N_2 glovebox. Mixtures of 3:2 w/w poly(3-hexylthiophene) (P3HT; Reike Metals):phenyl-C_{61}-butyric acid methyl ester (PCBM; Nano-C) were dissolved into chlorobenzene and then spin-coated onto the PEDOT:PSS surfaces to create film layers of 80 nm, as measured using a calibrated Dektak surface profilometer. For some of the devices, nitrobenzene was added to the spin-coating mixture directly before spin coating. Next, the samples were moved to a high vacuum chamber, where Ca/Ag electrodes were thermally evaporated through a shadow mask. All subsequent heating and measurement using the solar simulator were performed in the glovebox.

Samples for the washing experiments and reflectometry experiments were prepared on either cleaned glass slides or on silicon wafers with a native oxide layer. The cleaning steps were the same as described above. PEDOT:PSS was spin-coated on to the substrate followed by either P3HT or a mixture of P3HT and PCBM. The layered films were heated in the glovebox using a calibrated hot plate. The washing was performed by covering the entire film with chlorobenzene and then spinning the film. This process was repeated three to five times to ensure that any polymer not physically or chemically bound to the surface was washed away. Washing by soaking in an ultrasonic bath of chlorobenzene was also carried out, but gave the same contact angle results as those presented in this paper for the samples washed by spin-coating.

Device Measurements: AM1.5 light was provided by a filtered Xe lamp. The light intensity was calibrated using a Si photodiode but no mismatch factor was applied to the measurements. The *J–V* measurements were performed using a Keithley 2420 source measurement unit.

Contact Angle Measurements: Contact angle measurements were performed on a leveled goniometer stage. A droplet of H_2O was placed on the sample surface and then the contact angle was measured using a height-adjusted microscope camera and angle-determination software.

XANES Measurements: X-ray absorption near edge structure (XANES) data were taken at beam line 4.0.2 of the Advanced

Light Source synchrotron at the Lawrence Berkeley National Laboratory. The incident beam energy was scanned in increments of 0.5 eV in the energy range below the carbon K-edge from 250 to 275 eV, in 0.1 eV increments over the near-edge region from 275.1 to 300 eV, in increments of 0.2 eV from 300.2 to 330 eV and in increments of 0.5ÂăeV in the featureless region from 330.5 to 360 eV. The slit settings were reduced to 20Âăμm / 20Âăμm and the incident beam was defocused to a spot size of 1Âămm^2 to avoid radiation damage to the film samples. The incident beam intensity I_0 was measured with a 95% transmissive gold grid after the refocusing mirror, and the total electron yield (TEY) was measured with a Photonis Channeltron Electron Multiplier (model CEM 4716). A custom-designed superconducting tunnel junction X-ray spectrometer[53] was used to simultaneously record the X-ray fluorescence from them sample for each incident energy, and the intensity of the carbon K line used as a measure of the partial fluorescence yield (PFY). Both TEY and PFY signals were normalized by I_0 and set to unity in the flat region of 350 to 360 eV above the absorption features. Offset voltages were carefully zeroed so that the spectra not contain any of the structure in I_0 due to a small carbon contamination of the monochromator.

Neutron Scattering Measurements: Neutron Reflectometry Measurements: The properties of the thin-film layers of samples of PEDOT:PSS and/or P3HT spin-coated onto silicon wafer substrates and subjected to various heat and solvent treatments were determined by neutron reflectometry. The neutron reflectometry measurements were carried out using the Surface Profile Analysis Reflectometer (SPEAR) at the Manuel Lujan Jr. Neutron Scattering Center at the Los Alamos National Laboratory. A collimated neutron beam was directed at a sample at an incident angle of θ. The reflectivity *R*, defined as the ratio of the intensity of the specularly reflected neutron beam to that of the incident beam, was measured as a function of the momentum change perpendicular to the surface, $Q_z = (4\pi \sin\theta)/\lambda$, also known as the momentum transfer vector. Here λ is the wavelength of the neutrons. The measured reflectivity was fit to a slab model, in which the sample film was assumed to consist of a series of *n* parallel layers, where layer *i* has a thickness d_i and constant scattering length density (SLD) ρ_i, sandwiched between super- (air) and subphases (silicon) of infinite extent. Interlayer "roughness" $\sigma_{i,i+1}$, which could include contributions from actual roughness between layers or from interlayer mixing, was accounted for by an error function SLD profile centered at the interface connecting the SLDs of the adjacent layers *i* and $(i+1)$. Model fitting to the measured data for $\log R$ vs Q_z was carried out with the Levenberg-Marquardt nonlinear least-squares method using the `MOTOFIT` program[54], in which the reflectivity profile is calculated using the Abeles matrix method[55]. The scattering length densities of air, the silicon substrate, and native oxide layer on the substrate were taken to be $\rho_{air} = 0$, $\rho_{Si} = 2.07 \times 10^{-6}\ ^{-2}$, and $\rho_{SiO_2} = 3.47 \times 10^{-6}\ ^{-2}$, respectively.[54] For simplicity, the roughnesses above the Si and SiO_2 layers were assumed to be zero.

Acknowledgements

This work was supported by the US Department of Energy EERE Solar America Initiative under Contract No. DE-FG36-08GO18018. The thank LANL for neutron reflectometry measurement time at the LANSCE-SPEAR facility and measurement help obtained from Erik Watkins and Jarek Majewski. We thank the ALS for providing beam time. Part of this work was performed under the auspices of the U.S. Department of Energy by Lawrence Livermore National Laboratory under Contract DE-AC52-07NA27344.

References

[1] M. Osborn, *New polymers push Solarmers OPV efficiency to record 8.13 percent*, www.pv-tech.org, **2010**.

[2] H. Hoppe, N. S. Sariciftci, *J. Mater. Chem.* **2006**, *16*, 45–61.

[3] G. Li, V. Shrotriya, Y. Yao, J. S. Huang, Y. Yang, *J. Mater. Chem.* **2007**, *17*, 3126–3140.

[4] A. J. Moulé, K. Meerholz, *Adv. Funct. Mater.* **2009**, *19*, 3028–3036.

[5] T. Erb, U. Zhokhavets, G. Gobsch, S. Raleva, B. Stuhn, P. Schilinsky, C. Waldauf, C. J. Brabec, *Adv. Funct. Mater.* **2005**, *15*, 1193–1196.

[6] V. D. Mihailetchi, H. X. Xie, B. de Boer, L. J. A. Koster, P. W. M. Blom, *Adv. Funct. Mater.* **2006**, *16*, 699–708.

[7] X. N. Yang, J. Loos, S. C. Veenstra, W. J. H. Verhees, M. M. Wienk, J. M. Kroon, M. A. J. Michels, R. A. J. Janssen, *Nano Lett.* **2005**, *5*, 579–583.

[8] G. Greczynski, T. Kugler, M. Keil, W. Osikowicz, M. Fahlman, W. R. Salaneck, *J. Elect. Spectros. Rel. Phenom.* **2001**, *121*, 1–17.

[9] S. Kirchmeyer, M. Reuter, *J. Mater. Chem.* **2005**, *15*, 2077–2088.

[10] A. M. Nardes, M. Kemerink, R. A. J. Janssen, J. A. M. Bastiaansen, N. M. M. Kiggen, B. M. W. Langeveld, A. van Breemen, M. M. de Kok, *Adv. Mater.* **2007**, *19*, 1196–1200.

[11] A. M. Nardes, M. Kemerink, R. A. J. Janssen, *Phys. Rev. B* **2007**, *76*, 085208–7.

[12] A. M. Nardes, M. Kemerink, M. M. de Kok, E. Vinken, K. Maturova, R. A. J. Janssen, *Org. Electron.* **2008**, *9*, 727–734.

[13] Y. Kim, A. M. Ballantyne, J. Nelson, D. D. C. Bradley, *Org. Electron.* **2009**, *10*, 205–209.

[14] J. Hwang, F. Amy, A. Kahn, *Org. Electron.* **2006**, *7*, 387–396.

[15] C. Tengstedt, W. Osikowicz, W. R. Salaneck, I. D. Parker, C. H. Hsu, M. Fahlman, *Appl. Phys. Lett.* **2006**, *88*, 053502.

[16] S. Braun, M. P. de Jong, W. Osikowicz, W. R. Salaneck, *Appl. Phys. Lett.* **2007**, *91*, 202108.

[17] M. C. Scharber, D. Wuhlbacher, M. Koppe, P. Denk, C. Waldauf, A. J. Heeger, C. L. Brabec, *Adv. Mater.* **2006**, *18*, 789–794.

[18] M. Gross, D. C. Muller, H. G. Nothofer, U. Scherf, D. Neher, C. Brauchle, K. Meerholz, *Nature* **2000**, *405*, 661–665.

[19] J.-S. Kim, R. H. Friend, I. Grizzi, J. H. Burroughes, *Appl. Phys. Lett.* **2005**, *87*, 023506.

[20] A. B. D. Cassie, S. Baxter, *Trans. Faraday Soc.* **1944**, *40*, 546–551.

[21] S. K. M. Jonsson, M. P. de Jong, L. Groenendaal, W. R. Salaneck, M. Fahlman, *J. Phys. Chem. B* **2003**, *107*, 10793–10800.

[22] D. Schmeisser, M. Tallarida, K. Henkel, K. Müller, D. Mandal, D. Chumakov, E. Zschech, *Mater. Sci. Pol.* **2009**, *27*, 141–157.

[23] National Institute of Standards and Technology (NIST) Center for Neutron Research, Scattering Length Density Calculator: http://www.ncnr.nist.gov/resources/sldcalc.html.

[24] O. Tal, W. Gao, C. K. Chan, A. Kahn, Y. Rosenwaks, *Appl. Phys. Lett.* **2004**, *85*, 4148–4150.

[25] D. Cahen, A. Kahn, *Adv. Mater.* **2003**, *15*, 271–277.

[26] P. Zacharias, M. C. Gather, M. Rojahn, O. Nuyken, K. Meerholz, *Angew. Chem. Int. Ed.* **2007**, *46*, 4388–4392.

[27] M. Fahlman, A. Crispin, X. Crispin, S. K. M. Henze, M. P. d. Jong, W. Osikowicz, C. Tengstedt, W. R. Salaneck, *J. Phys.: Condens. Matter* **2007**, 183202.

[28] S. Braun, W. R. Salaneck, M. Fahlman, *Adv. Mater.* **2009**, *21*, 1450–1472.

[29] K. Peter, C. Volhardt, N. E. Schore, *Organic Chemistry: Structure and Function*, Freeman and Co., **2003**.

[30] M. M. Bouman, E. E. Havinga, R. A. J. Janssen, E. W. Meijer, *Molecular Crystals and Liquid Crystals Science and Technology Section a-Molecular Crystals and Liquid Crystals* **1994**, *256*, 439–448.

[31] R. Osterbacka, C. P. An, X. M. Jiang, Z. V. Vardeny, *Science* **2000**, *287*, 839–842.

[32] K. H. Yim, G. L. Whiting, C. E. Murphy, J. J. M. Halls, J. H. Burroughes, J. S. Kim, *Adv. Mater.* **2008**, *20*, 3319–3324.

[33] C. Y. Kao, B. Lee, L. S. Wielunski, M. Heeney, I. McCulloch, E. Garfunkel, L. C. Feldman, V. Podzorov, *Advanced Functional Materials* **2009**, *19*, 1906–1911.

[34] W. Ma, C. Yang, X. Gong, K. Lee, A. J. Heeger, *Adv. Funct. Mater.* **2005**, *15*, 1617–1622.

[35] F. Padinger, R. S. Rittberger, N. S. Sariciftci, *Adv. Funct. Mater.* **2003**, *13*, 85–88.

[36] F. L. Zhang, K. G. Jespersen, C. Bjorstrom, M. Svensson, M. R. Andersson, V. Sundstrom, K. Magnusson, E. Moons, A. Yartsev, O. Inganas, *Adv. Funct. Mater.* **2006**, *16*, 667–674.

[37] J. Peet, J. Y. Kim, N. E. Coates, W. L. Ma, D. Moses, A. J. Heeger, G. C. Bazan, *Nat. Mater.* **2007**, *6*, 497–500.

[38] A. J. Moulé, K. Meerholz, *Adv. Mater.* **2008**, *20*, 240–245.

[39] V. D. Mihailetchi, L. J. A. Koster, J. C. Hummelen, P. W. M. Blom, *Phys. Rev. Lett.* **2004**, *93*, 216601.

[40] P. Peumans, S. Uchida, S. R. Forrest, *Nature* **2003**, *425*, 158–162.

[41] A. W. Hains, A. B. F. Liu, J. Martinson, M. D. Irwin, T. J. Marks, *J. Mater. Chem.* **2010**, *20*, 595–606.

[42] J. S. Huang, G. Li, Y. Yang, *Appl. Phys. Lett.* **2005**, *87*, 112105.

[43] Y. Kim, S. A. Choulis, J. Nelson, D. D. C. Bradley, S. Cook, J. R. Durrant, *Appl. Phys. Lett.* **2005**, *86*, 063502.

[44] M. Reyes-Reyes, K. Kim, D. L. Carroll, *Appl. Phys. Lett.* **2005**, *87*, 083506.

[45] B. Xue, B. Vaugham, C.-H. Poh, K. B. Burke, L. Thomsen, A. Stapleton, X. Zhou, G. W. Bryant, W. Belcher, P. C. Dastoor, *J. Phys. Chem. C (in Press)* **2010**.

[46] A. Gadisa, W. Mammo, L. M. Andersson, S. Admassie, F. Zhang, M. R. Andersson, O. Inganas, *Adv. Funct. Mater.* **2007**, *17*, 3836–3842.

[47] X. Y. Cheng, Y. Y. Noh, J. P. Wang, M. Tello, J. Frisch, R. P. Blum, A. Vollmer, J. P. Rabe, N. Koch, H. Sirringhaus, *Adv. Funct. Mater.* **2009**, *19*, 2407–2415.

[48] S. Cho, J. Yuen, J. Y. Kim, K. Lee, A. J. Heeger, *Appl. Phys. Lett.* **2007**, *90*, 063511.

[49] D. S. Germack, C. K. Chan, R. J. Kline, D. A. Fischer, D. J. Gundlach, M. F. Toney, L. J. Richter, D. M. DeLongchamp, *Macromolecules* **2010**, *43*, 3828–3836.

[50] M. Campoy-Quiles, T. Ferenczi, T. Agostinelli, P. G. Etchegoin, Y. Kim, T. D. Anthopoulos, P. N. Stavrinou, D. D. C. Bradley, J. Nelson, *Nat. Mater.* **2008**, *7*, 158–164.

[51] S. van Bavel, E. Sourty, G. de With, K. Frolic, J. Loos, *Macromolecules* **2009**, *42*, 7396–7403.

[52] Z. Xu, L. M. Chen, G. W. Yang, C. H. Huang, J. H. Hou, Y. Wu, G. Li, C. S. Hsu, Y. Yang, *Adv. Funct. Mater.* **2009**, *19*, 1227–1234.

[53] S. Friedrich, O. B. Drury, S. J. George, S. P. Cramer, *Nuc. Inst. & Meth. Phys. Res.* **2007**, *582*, 187–189.

[54] A. Nelson, *J. Appl. Cryst.* **2006**, *39*, 273–276.

[55] O. S. Heavens, *Optical Properties of Thin Solid Film*, Dover, New York, **1991**.

Supporting Information for “The Consequences of Interface Mixing on Organic Photovoltaic Device Characteristics”

David M. Huang, Scott A. Mauger, Stephan Friedrich,
Simon J. George, Daniela Dimitriu LaGrange, Sook Yoon, and Adam J. Moulé

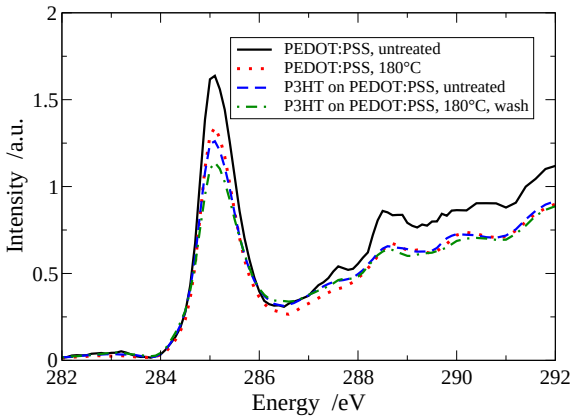

Figure S1: X-ray absorption near edge structure (XANES) spectra of the carbon K edge of untreated PEDOT:PSS (solid line), PEDOT:PSS heated to 180°C (dotted line), untreated P3HT on PEDOT:PSS (dashed line). and P3HT on PEDOT:PSS that was heated to 180°C and then washed with chlorobenzene (dot-dashed line).

References

[] T. A. Chen, X. M. Wu, R. D. Rieke, *Journal of the American Chemical Society* **1995**, *117*, 233–244.

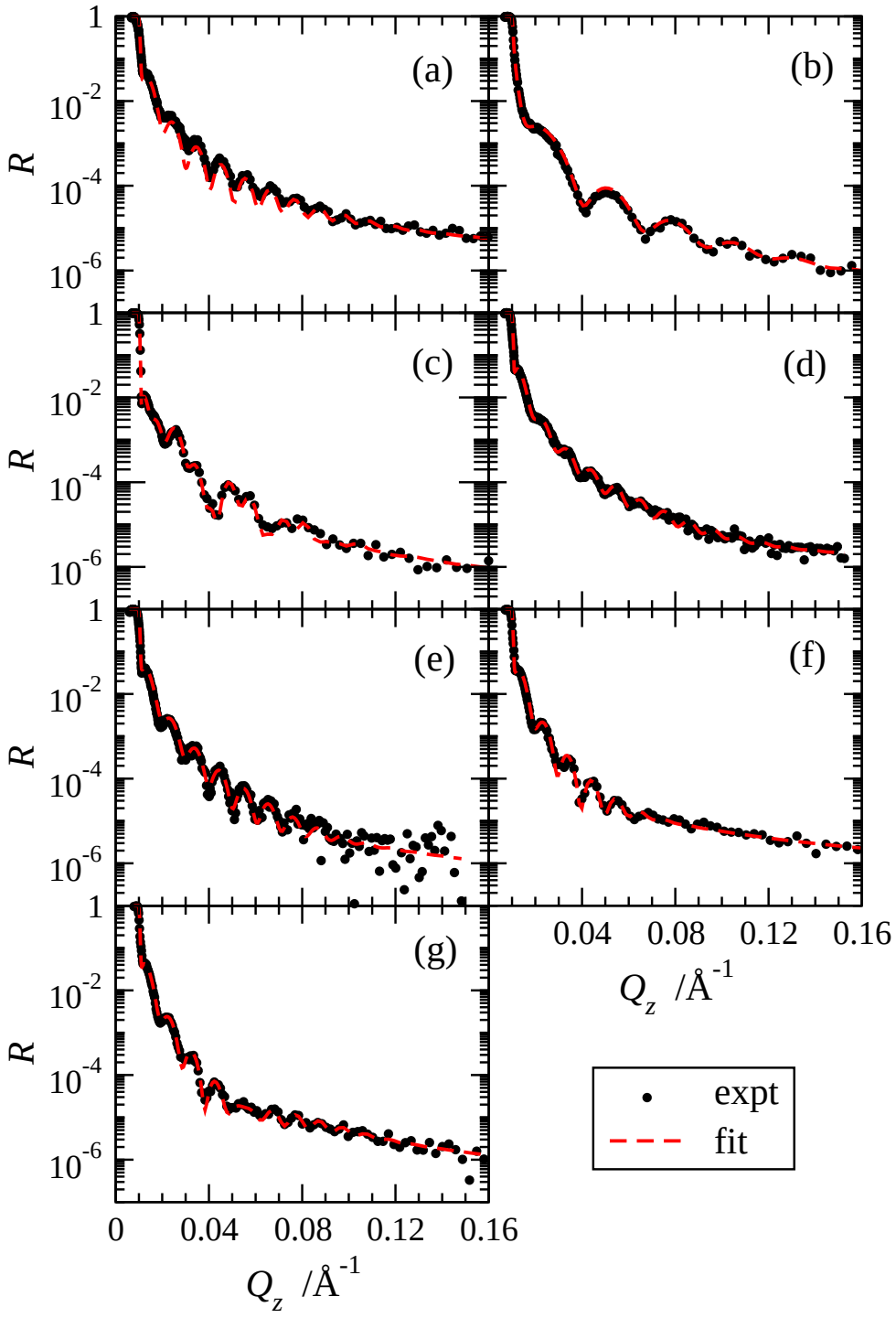

Figure S2: Reflectivity R vs momentum transfer vector Q_z from measurements (points) and fits (lines) of various samples on silicon wafers: (a) PEDOT:PSS, (b) P3HT, (c) unwashed P3HT on PEDOT:PSS, and P3HT on PEDOT:PSS heated then washed with chlorobenzene, with heat treatment temperature of (d) room temperature, (e) 150°C, (f) 180°C, and (g) 210°C.

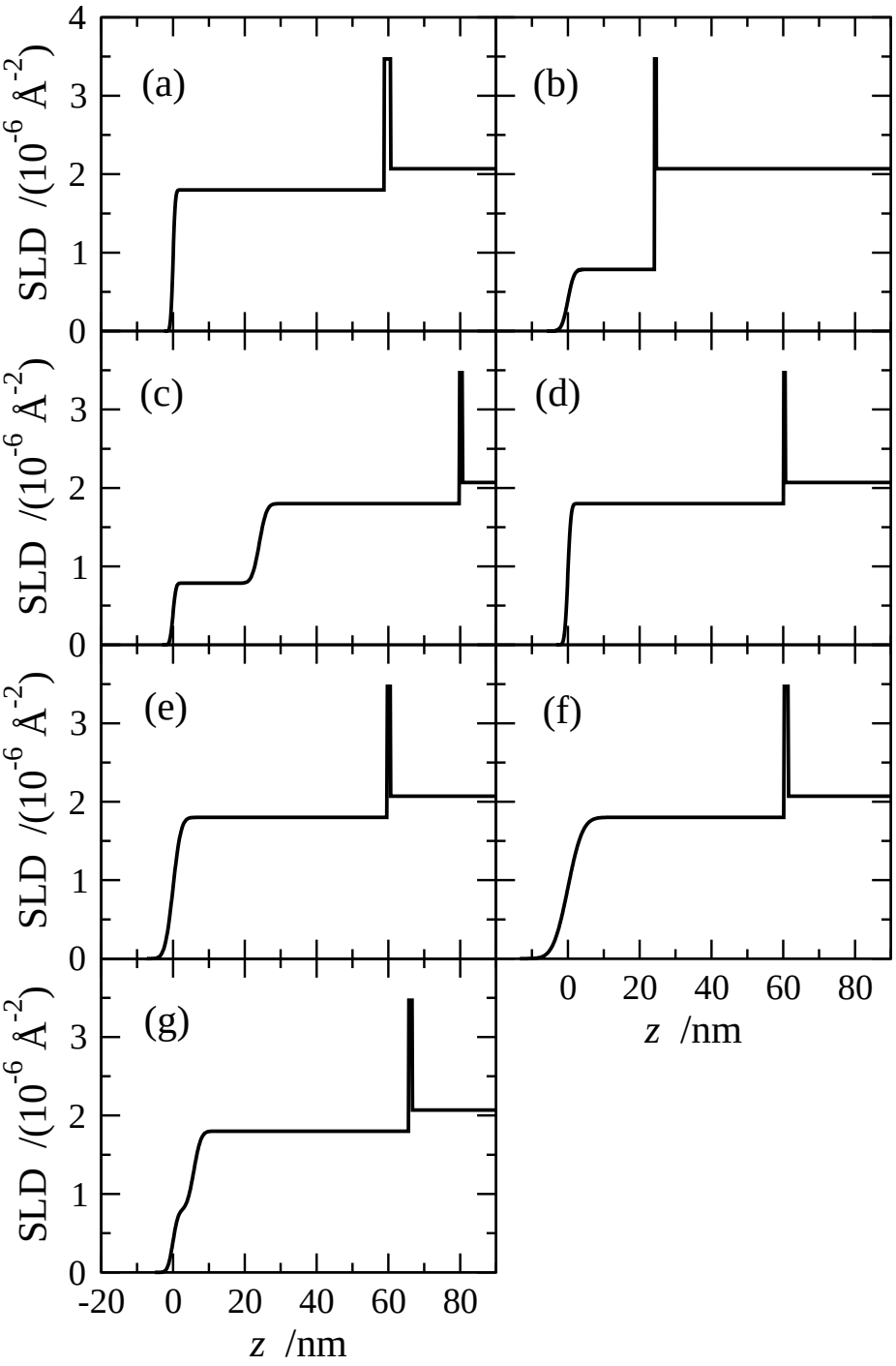

Figure S3: Scattering length density SLD vs distance from the top surface of samples from fits to the measured reflectivity data in Figure **??**: (a) PEDOT:PSS, (b) P3HT, (c) unwashed P3HT on PEDOT:PSS, and P3HT on PEDOT:PSS heated then washed with chlorobenzene, with heat treatment temperature of (d) room temperature, (e) 150°C, (f) 180°C, and (g) 210°C.

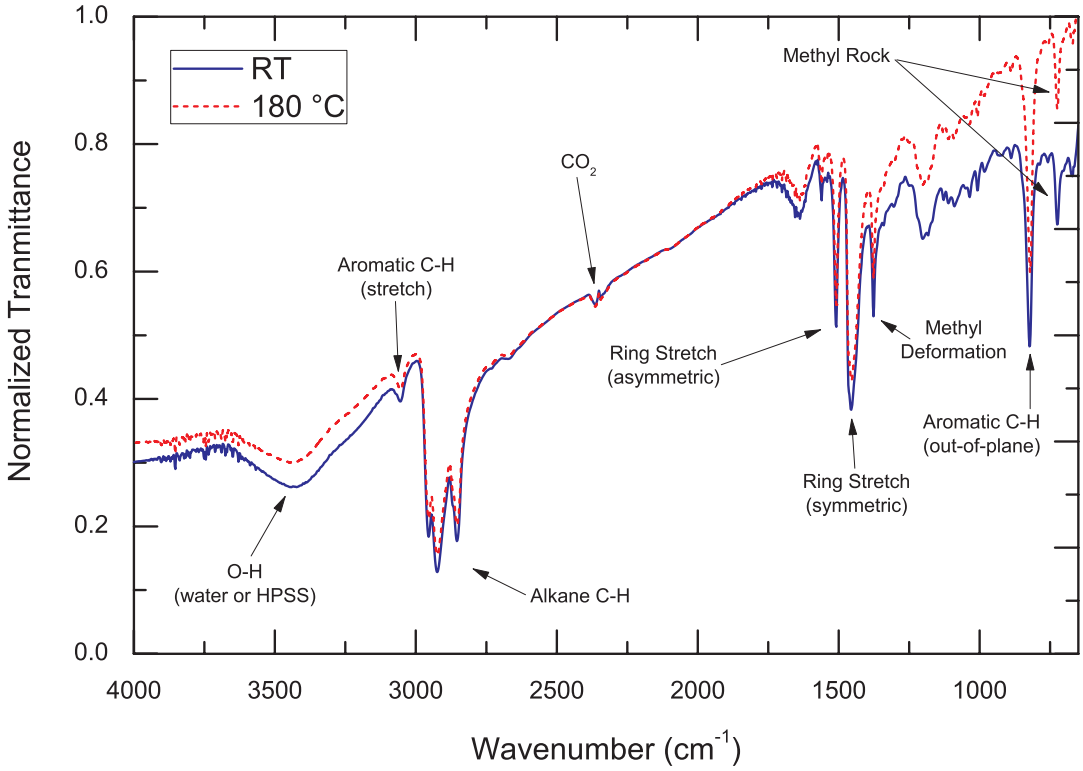

Figure S4: FTIR spectra of mixed P3HT/PEDOT:PSS before (line) and after (dotted line) heat treatment at 180°C. The P3HT and dried PEDOT:PSS were mixed as powder samples in a mortar and pestle with KBr. Half of the samples was subsequently heated to 180°C. Then both samples were mechanically pressed and measured in transmission in the FTIR. The differences in the spectra come from sample geometry. There is no evidence of new peak formation or a change in the peak ratios. Assignments of the peaks were taken from Chen et. al.[**?**]

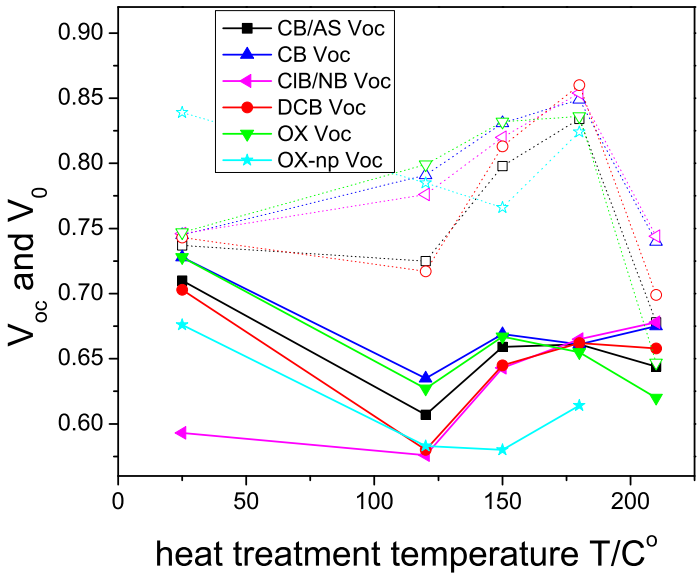

Figure S5: V_{oc} (filled shapes, solid lines) and V_0 (open shapes, dotted lines) versus heat treatment temperature for 3:2 P3HT:PCBM BHJ OPV devices with an active layer thickness of 80 nm. The devices were cast from 19:1 chlorobenzene (CB):anisole (AS) (squares), CB (up triangle), 19:1 CB:nitrobenzene (NB) (left triangle), 1,2 dichlorobenzene (DCB) (circle), orthoxylene (OX) (down tirangle), and preformed nanofibers of P3HT in OX (OX-np) (stars). As stated in the main text, the V_{oc} shows no consistant trend and is quite dependent on layer morphology. In contrast, V_0 shows a clear dependence on heat-treatment temperature. For most devices V_0 increases with increasing heat-treatment temperature with a maximum at 180°C. There are three exceptions. For the solvents CB/AS and DCB, the V_0 is lowest for heat-treatment at 120°C. This is because both AS and DCB are high boiling point solvents that evaporate slowly from the active layer. The presence of these solvents in the films causes the formation of large PCBM domains that greatly increase the dark current, lowering FF, V_{oc}, and V_0. The V_0 increases to the same value as the other devices with heating to 150°C because the formation of the interlayer reduces the dark current. The OX-np also has a much different dependence of V_0 on heat treatment temperature. For OX-np, V_0 is highest with no heat treatment and decreases to a minimum at 150°C. Finally the V_0 is (within error) the same as the other devices after heating to 180°C. This different dependence is because the P3HT nano fibers have poor electrical connectivity to each other after spin coating, so the dark current is quite low for the unheated sample. With heating the PCBM forms extended domains that transport charge efficiently between the electrodes, which greatly increase the dark current while reducing V_{oc}, V_0 and FF. The interlayer does not form until the higher temperature of 180°C because the P3HT nanofibers must melt before the interlayer is formed.

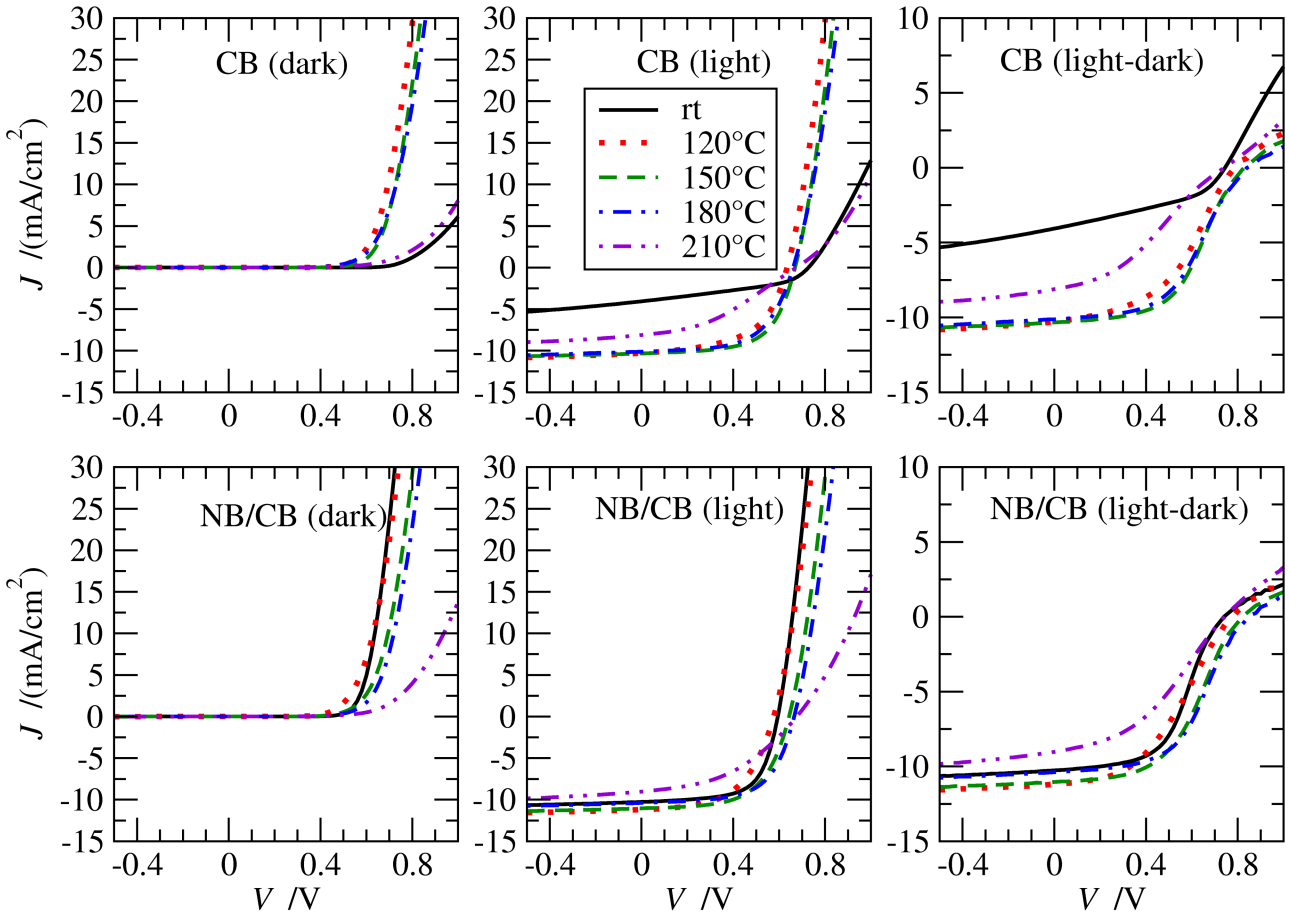

Figure S6: Dark (left), light (middle), and photocurrent (right) JV curves for 3:2 P3HT:PCBM BHJ devices that were cast from chlorobenzene (upper three panels) and 19:1 chlorobenzene:nitrobenzene (lower three panels). On each graph are depicted the heat treatments ranging from room temperature (solid line), 120°C (dotted line), 150°C (dashed line), 180°C (dash-dot line), and 210°C (dash-dot-dot line). Notice that reduction in the dark current for devices heat treated to 150°C and 180°C leads to increased photocurrent at higher applied potentials.